EVALUATING DUNE DELINEATION ON IMAGES FROM MARS. L. Bandeira[1], J. Saraiva[1], P. Pina[1] and J. S. Marques[2], [1]CERENA / IST (Av. Rovisco Pais, 1049-001 Lisboa, Portugal; lpcbandeira@ist.utl.pt), [2]ISR / IST (Av. Rovisco Pais, 1049-001 Lisboa, Portugal).

Introduction: Research into aeolian features on Mars has increased markedly with the availability of very high spatial resolution images of the surface [1]. Assessing the global distribution, shape and other characteristics of dunes can lead to an improved understanding of the interactions between the atmosphere and the surface of the planet [2]. The sheer quantity of data to be analyzed suggests that the use of automated methods can play an important role in fully exploiting the information that is being collected by automated probes. Thus, we have seen studies on temporal changes [3], determination of dune heights [4], morphologies [5] and spatial patterns [6], often considering analogies with terrestrial dunes. However, detailed automated dune delineation is seldom tackled – there is only one recent example [7], other than work produced by this team [8, 9]. In here, after a short reminder of our methodology, we present an evaluation of the results achieved, focused on the diverse types of dunes contained in the dataset employed.

Methodology: The strategy followed in our approach is based on the tiling of an image into relatively small square cells, which are then classified. The use of a simple geometric shape makes the analysis very fast and leads to a non-iterative solution which is compatible with the large amount of data to be processed. This task is done through the extraction and analysis of local information (image features) along the regular grid of the tiled image. To benefit from context and diminish dependence on specific factors such as illumination, an aggregation of the local features of neighbouring cells is performed within a block, i.e., a region constituted by 3×3 cells, and that constitutes the detection window of the methodology [10]. This block window is moved along the whole grid with a cell-sized step in order to analyse the complete image. For the full mathematical formalism and additional details, we advise readers to consult our previous publication [9].

The different sets of features and classifiers tested have mostly conducted to very good results, when applied to barchan and barchanoid dunes. Thus, we decided to enlarge the field of application to other types of dunes found on the surface of Mars, employing the combination features/classifier that has previously yielded the best results.

Dataset: Our dataset for this work is constituted by 160 MOC N/A images distributed around the surface of the planet and with a good temporal coverage, subject to image availability. All have a spatial resolution better than 6.80 m/pixel, down to 1.45 m/pixel. These images were visually analysed, in order to construct a ground-truth for each of them by manually drawing the contours of the dunes on-screen. To compare the ground-truth with the result produced by the automated classifier, both must be in the same format. Thus, we had to tile each ground-truth exactly like its corresponding original image. Furthermore, we had to consider three types of cells: 'non-dune', 'dune' and 'unclassifiable'. To assign one of these labels to a cell, we computed the area occupied by dune terrain in the block from which it is the centre: if this area is less than 10% of the number of pixels of the block, the cell is 'non-dune'; if it is higher than 30%, the cell is 'dune'; if the area is between 10 and 30%, any decision is ambiguous, so we decided not to classify it.

The images constituting the dataset include examples of the major types of dunes, according to the literature [11, 12]: barchan (BC), barchanoid (BN), transverse (TV), dome (DO), linear (LN), star (ST), sand sheet (SS) and other (OT) (Figure 1).

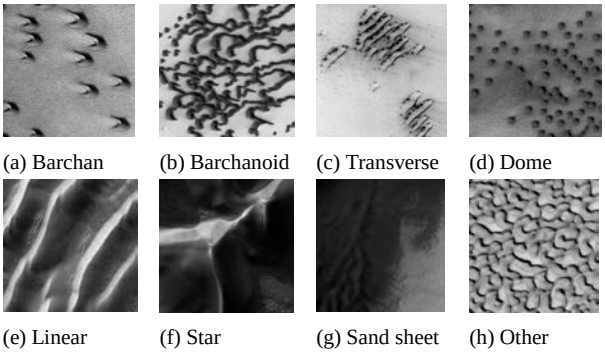

Figure 1: Examples of main Martian dune types from our dataset (the side of each square image is 2500 metres) [image credits: NASA/JPL/MSSS].

When translating the original grey-level images into a binary ground-truth, the eight types of dunes produced images with certain common geometric characteristics. This led us to consider another classification scheme, grouping the binary objects into four types of bulk shapes (Figure 2): 'isolated' (mainly barchans and domes); 'elongated' (mainly barchanoids, linear and transverse); 'compact' (sand sheets, and

dense combinations of other types) and 'compact with holes' (star and others).

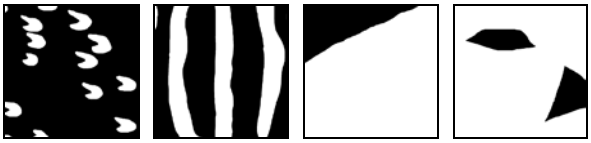

(a) Isolated (b) Elongated (c) Compact (d) Compact with holes

Figure 2: Examples of the four bulk shapes encountered in the binary ground-truth (the side of each square image is 2500 metres).

Results: The results we have obtained for the whole set of images confirm that this methodology is a valid contribution to the automated mapping of dune fields on remotely sensed images. There are 277,524 cells to be classified in the 160 images, and the average global probability of error is around 0.11. Moreover, we employed a cross-validation procedure where the dataset was divided in five groups, and each of those was used in turn to test the methodology (while the other four were, in each run, used for training). The five groups were built in such a way as to have a comparable number of positive 'dune' examples. The results for these five runs illustrate the robustness of the methodology: the lowest probability of error is less than 0.09, the highest is little over 0.14.

As stated above, some care was exercised to include in the set of images examples of most of the Martian dune types commonly recognized. This was done to try and evaluate the response of the methodology to the differing characteristics in shape, dimension and contiguity that they present. The results obtained considering the distribution of the dune types in the 160 images can be appreciated in Table I.

Table I – Performance of classifier by type of dunes.

	# images	*# 'dune' cells*	*# 'non-dune' cells*	p_{error}
Barchan	31	15,111	33,588	0.088
Barchanoid	43	24,889	47,624	0.067
Transverse	4	691	3,179	0.099
Dome	12	5,434	8,212	0.186
Linear	18	22,746	19,455	0.169
Star	2	2,167	1,290	0.209
Sand sheet	11	7,346	13,819	0.129
Other	39	33,645	38,328	0.110

The range of values again highlights the robustness of the methodology. Barchan and barchanoid types achieve the best performance with a probability of error below 0.09; on the other hand the star dunes, poorly represented, show the worst probability of error, but even this is only about 0.21.

For the four categories that resulted from the grouping of the ground-truth shapes, the results are very good and similar between types (Table II). The best result is about 0.10 for the 'compact with holes' and the worst is 0.12 for the 'elongated' type; these are very close to the average result obtained for the set of 160 images considered globally.

Table II – Performance of classifier by bulk shape of ground-truth.

	# images	*# 'dune' cells*	*# 'non-dune' cells*	p_{error}
Isolated	50	16,415	50,715	0.115
Elongated	53	42,137	56,495	0.115
Compact	29	26,393	26,228	0.108
Compact with holes	28	27,084	32,057	0.098

Conclusion: The main conclusion is that the performance of our methodology, based on gradient histograms coupled with a SVM classifier, can be considered very good: independently of the way in which the dataset is analysed (globally, by type of dune or bulk shape), the average probability of error is about 0.11. In 160 images only a handful present an error that can be considered high. Those images will be scrutinized in detail in order to understand where the classifier went wrong and improve its performance; ideas for future work include the extraction of other types of features and the use of a multi-scale strategy.

References: [1] Bourke MC et al (2010) *Geomorph, 121,* 1-14. [2] Fenton LK and Hayward RK (2010) *Geomorph, 121,* 98-121. [3] Silvestro S et al (2010) *GRL, 37,* L20203. [4] Bourke MC et al (2006) *Geomorph, 81,* 440-452. [5] Ewing RC et al (2006) *ESPL, 31,* 1176-1191. [6] Bishop MA (2010) *Geomorph, 120,* 186-194. [7] Chowdhury PR et al (2011) *JSTAEORS, 4,* 171-184. [8] Bandeira L et al (2010) *LNCS, 6112,* 306-315. [9] Bandeira L et al (2011) *GRSL, 8,* 626-630. [10] Dalal N and Triggs B (2005) *Proc. CVPR,* 886-893. [11] Mckee ED (1979) Univ. Press Pacific, Honolulu. [12] Hayward R et al (2007) *JGR, 112,* E1107.

Acknowledgments: Work supported by FCT (Portugal), through project ANIMAR (PTDC/CTE-SPA/110909). LB and JS acknowledge finantial support in the form of BPD and BD grants from FCT.